A Hybrid-Control Approach to the Parking Problem of a Wheeled Vehicle Using Limited View-Angle Visual Feedback

Pierpaolo Murrieri Daniele Fontanelli Antonio Bicchi

Index Terms— **Parking of Wheeled Robots, Visual Servoing, Hybrid Control, Nonholonomic Systems.**

Abstract— **In this paper we consider the mobile robot parking problem, i.e. the stabilization of a wheeled vehicle to a given position and orientation, using only visual feedback from low-cost cameras. The practically most relevant problem of keeping the tracked features in sight of the camera while maneuvering to park the vehicle is taken into account. This constraint, often neglected in the literature, combines with the nonholonomic nature of the vehicle kinematics in a challenging controller design problem. We provide an effective solution to such problem by using a combination of previous results on non-smooth control synthesis and recently developed hybrid control techniques. Simulations and experimental results on a laboratory vehicle are reported, showing the practicality of the proposed approach.**

I. Introduction

Wheeled vehicles have a wide range of applications, both in indoor and outdoor environments, and represent one of the areas with larger potential for advanced robotics. A very important trend in research related to mobile robots is concerned with their sensorization, and in particular with the tradeoffs between effectiveness and cost of different possible sensorial apparatuses. This paper deals with the problem of using economic, off-the-shelf cameras to solve the complex problem of parking (or "docking") a wheeled vehicle to a given desired position and orientation in the plane where it moves.

In the literature, problems concerning mobile robots stabilization have received wide attention. Set-point stabilization (a problem that for a few years challenged the research community, due to the famous theorem of Brockett on smooth stabilization [1]), has been solved (assuming full state information) among others by [2], [3], [4], [5] using time-varying control laws, and by e.g. [6], [7] by non-smooth feedback control laws.

In practical applications of automated vehicles, however, one is confronted with the problem of knowing the current position and orientation of the vehicle only through indirect measurements by available sensors. Although much work has been done on techniques for vehicle localization based on combinations of sensory information (odometry, laser range finders, cameras, etc.), very little is known about the real time connection of a localization algorithm and a feedback control law. In this paper, we consider a vehicle equipped only with a fixed monocular camera, and control laws that close the feedback loop directly at the sensor level, i.e. using information available from 2D images, with very limited information on the environment.

Previous work on visual servoing of mobile vehicles has considered the case of a camera that can move independently from the vehicle ([8]), or is carried by an articulated arm mounted on the robot ([9]), or, finally, it is simply fixed to the vehicle's chassis ([10], [11]). In the latter papers, a feedback control law stabilizing the vehicle posture by using visual information only was solved. Furthermore, [11] considers the practically most relevant problem of keeping the features to be tracked within sight of a limited aperture camera while the vehicle maneuvers to park, and proposes a heuristic correction to the control law that solves the problem in many cases. It is to be noted that, although different sensors (such as some models of laser range finders, or omidirectional cameras, or again pan-tilt heads) may not be affected by view-angle limitations, these are typically some orders of magnitude more expensive than the conventional cameras we consider, which are readily available even in the consumer market.

Specific problems related to the limited field-of-view (FOV) have been considered in some detail for robot arm control (see e.g. [12]). For wheeled mobile robots, [9] proposes a solution relying on the extra d.o.f.'s availed by an articulated arm on-board. Unfortunately, economy considerations will in most cases only allow the camera to be rigidly fixed to the vehicle: in this case, the FOV constraint combines with the nonholonomic nature of the vehicle kinematics in a challenging controller design problem.

In this paper, we provide an effective solution to the problem with a fixed camera on-board the vehicle, by using a combination of previous results on non-smooth control synthesis and recently developed hybrid control techniques. Simulations and experimental results on a laboratory vehicle are reported, showing the practicality of the proposed approach.

II. Localization of the Robot

Visual servoing techniques use visual information directly, by the computation of an image error signal, or indirectly, by the evaluation of the state of the system. These two approaches were classified by Weiss in 1984 as *Image Based Visual*

Manuscript submitted January 2003. Support from EC contract IST2001–37170 RECSYS, CNR contract C00E714–001, ASI contract I/R/124/02 "TEMA", MURST grants "Mistral" and "Matrics".

Authors are with the Interdept. Research Center "Enrico Piaggio", University of Pisa, via Diotisalvi, 2, 56100 Pisa, Italy. Phone: +39050553639. Fax:+39050550650. E–mail: murrieri,fontanelli,bicchi@piaggio.ccii.unipi.it

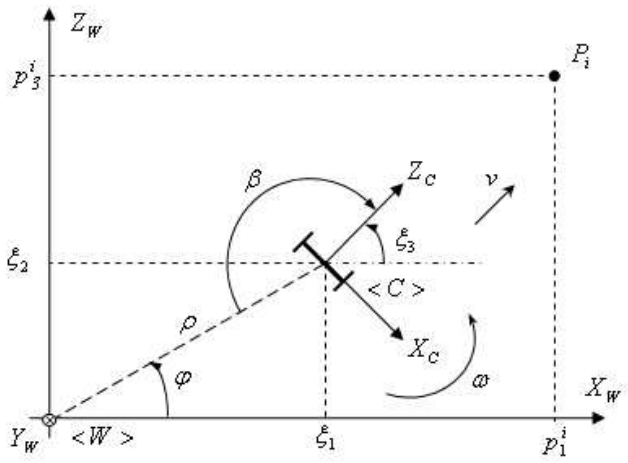

Fig. 1. Fixed frame $< W >$, camera frame $< C >$, and relative coordinates (ξ_1, ξ_2, ξ_3) and (ρ, ϕ, β)

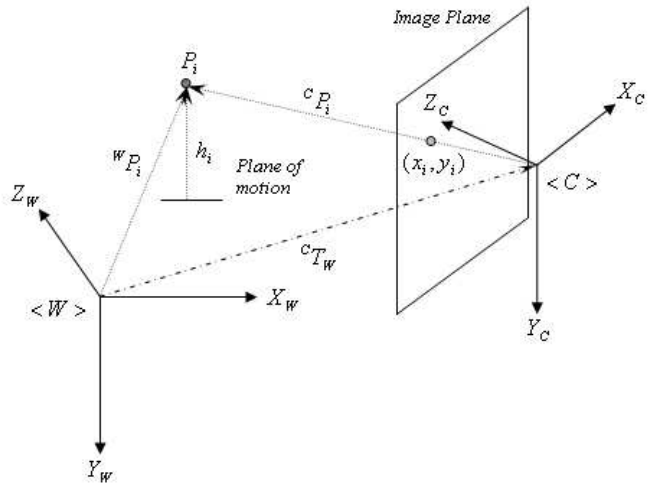

Fig. 2. Fixed frame $< W >$, camera frame $< C >$ and relative feature coordinates.

Servoing (IBVS) and *Position Based Visual Servoing* (PBVS), respectively. Indeed, these two schemes should be regarded as the end-points of a range of different possibilities, whereby the raw sensorial information is gradually abstracted away to a more structured representation using some knowledge of the robot-environment model (a scheme which is roughly half-way between IBVS and PBVS was used e.g. in [11]).

IBVS and other sensor-level control schemes have several advantages, such as robustness (or even insensitivity) to modeling errors and hence suitability to unstructured scenes and environments. On the other hand, PBVS and in general higher-level control schemes also have important attractive features. Using the PBVS approach, for instance, the control law can be synthesized in the usual working coordinates for the robot, and thus usually a simpler synthesis is made possible. Furthermore, abstracting sensor information to a higher level of representation allows using different sensorial sources. In our example of a camera mounted on a mobile robot, for instance, the synergistic use of odometry and visual feedback is only possible if these information can be described in the same coordinate frame, where they can be fused coherently. These latter considerations motivate our usage in this paper of the PBVS approach, which is detailed in what follows.

Let's consider a moving camera frame $< C >$ fixed on the mobile robot with the origin in the camera pinhole, with the Z_c axis directed along the camera optical axis and with the Y_c axis perpendicular to the plane of motion and passing through the middle point of the unicycle axle (see fig. 1). From the current image, $n \geq 2$ characteristic points (features) are selected with coordinates in the camera frame ${}^CP_i = {}^C[p_1^i, p_2^i, p_3^i]^T$. Under the assumption that the motion is constrained on the ${}^CX \times {}^CZ$ plane, the coordinates ${}^cp_2^i = h_i$ of each feature are constant and represent the height of the feature on the plane of motion. For simplicity's sake, we assume that the height of the features is known (the assumption can be avoided by e.g. using multiple views of the same features from different positions of the camera and a suitable calibration procedure beforehand, or by using a stereo camera pair). In this case, using only camera measurements and calibration parameters, feature coordinates ${}^CP_i$ can be evaluated by standard methods (see e.g. [13]).

Consider now a fixed frame $< W >$ whose origin is coincident with the origin of $< C >$ when the robot is in the desired final configuration, and with $X_w = Z_c$ and $Y_w = Y_c$. Let ${}^W\xi = {}^W[\xi_1, \xi_2, \xi_3]^T \in \mathbb{R}^2 \times S$ denote the robot posture. More precisely, (ξ_1,ξ_2) are the cartesian coordinates of the middle point of the unicycle axle, and ξ_3 is the orientation of the unicycle between the Z_c axis and the X_w axis, as represented in figure 1. From this initial position of the vehicle an image of a portion of the scene in view is grabbed. Let ${}^WP_i = {}^W[p_1^i, p_2^i, p_3^i]^T$ be the i–th feature coordinates with respect to $< W >$. All the features are motionless in $< W >$.

The current position of the feature ${}^CP_i$ in camera frame is related to ${}^WP_i$ in the fixed frame by a rigid-body motion (see fig. 2).

By some standard geometric calculations, a relationship among the feature coordinates in the fixed and moving frames, and the robot posture, is obtained as

$$ {}^C \begin{bmatrix} p_1^i \\ p_3^i \end{bmatrix} = \begin{bmatrix} {}^Wp_3^i & {}^Wp_1^i & 1 & 0 \\ -{}^Wp_1^i & {}^Wp_3^i & 0 & 1 \end{bmatrix} b, \qquad (1) $$

with

$$ b = \begin{bmatrix} -\cos\xi_3 \\ \sin\xi_3 \\ \xi_2\cos\xi_3 - \xi_1\sin\xi_3 \\ -\xi_1\cos\xi_3 - \xi_2\sin\xi_3 \end{bmatrix} \qquad (2) $$

Equation (1) can be regarded as providing two nonlinear scalar equations in the 3 unknowns (ξ_1, ξ_2, ξ_3), for each feature observed in the current and reference images.

Strictly speaking, equations of this type could provide a solution for the vehicle position even with just two features, provided that some geometric conditions are fulfilled (the straight line passing through the two points corresponding to the features under consideration should not be perpendicular to the plane of motion of the vehicle). However, more robustness is achieved by using a larger number of features. Assuming a

number $n \geq 4$ of features, the actual unknown position and orientation ${}^W\xi$ of the unicycle can be evaluated by solving for b (in a least-squares sense) the linear system

$$ {}^C \begin{bmatrix} p_1^1 \\ p_3^1 \\ \vdots \\ p_1^n \\ p_3^n \end{bmatrix} = \begin{bmatrix} {}^W p_3^1 & {}^W p_1^1 & 1 & 0 \\ -{}^W p_1^1 & {}^W p_3^1 & 0 & 1 \\ \vdots & \vdots & \vdots & \vdots \\ {}^W p_3^n & {}^W p_1^n & 1 & 0 \\ -{}^W p_1^n & {}^W p_3^n & 0 & 1 \end{bmatrix} b. \qquad (3) $$

This problem is solvable for each position of the vehicle in $\mathbb{R}^2 \times S$, just provided that the $n \geq 4$ features don't belong to a single plane perpendicular to the plane of motion. Once b is estimated, the values of (ξ_1, ξ_2, ξ_3) can be readily obtained by inverting (2).

III. Visual-Servoing with Omnidirectional Sight

We start our development considering first the case that no view-angle limitation is present for the camera, as it happens with some recently proposed devices (see e.g. [14]), and that a single feature has to be tracked which corresponds to exactly the desired position for the robot.

Consider for this problem a set of new coordinates, which is better suited to describe the angle by which the feature is observed from the vehicle, described by $\Phi : \mathbb{R}^2 \times S \rightarrow \mathbb{R}^+ \times S^2$ with (see fig. 1)

$$ \begin{bmatrix} \rho \\ \phi \\ \beta \end{bmatrix} = \Phi(\xi) = \begin{bmatrix} \sqrt{{\xi_1}^2 + {\xi_2}^2} \\ \arctan(\frac{\xi_2}{\xi_1}) \\ \pi + \arctan(\frac{\xi_2}{\xi_1}) - \xi_3 \end{bmatrix}. \qquad (4) $$

Observe that this change of coordinates is a diffeomorphism everywhere except at the origin of the plane (exactly where the feature point is), as discussed in more detail in [6]. The dynamics of the unicycle in the new coordinates are easily obtained as

$$ \begin{bmatrix} \dot\rho \\ \dot\phi \\ \dot\beta \end{bmatrix} = \begin{bmatrix} -\rho\,\cos\beta \\ \sin\beta \\ \sin\beta \end{bmatrix} u + \begin{bmatrix} 0 \\ 0 \\ -1 \end{bmatrix} \omega, \qquad (5) $$

where we let $u = \frac{v}{\rho}$. A continuous, time-invariant control law can in principle stabilize system (5) – indeed, the two control vector fields are now linearly dependent at the origin, thus making Brockett's negative result [1] unapplicable.

Consider the candidate Lyapunov function (proposed in [6]) $V = \frac{1}{2}(\rho^2 + \phi^2 + \lambda\beta^2)$, with $\lambda > 0$ a free parameter to be used in the following controller design. One has

$$ \dot V = -\rho^2 \cos\beta\, u + \phi \sin\beta\, u + \lambda\beta \sin\beta\, u - \lambda\beta\omega, \qquad (6) $$

and, by setting

$$ \begin{aligned} u &= \cos\beta, \\ \omega &= \tfrac{\phi \sin\beta \cos\beta + \lambda\beta \sin\beta \cos\beta}{\lambda\beta} + \beta, \end{aligned} \qquad (7) $$

one gets $\dot V = -\rho^2 \cos^2\beta - \lambda\beta^2 \leq 0$. The controlled dynamics with this choice are

$$ \begin{bmatrix} \dot\rho \\ \dot\phi \\ \dot\beta \end{bmatrix} = \begin{bmatrix} -\rho\,\cos^2\beta \\ \sin\beta\cos\beta \\ -\frac{\phi\ \sin 2\beta}{2\lambda\beta} - \beta \end{bmatrix}. \qquad (8) $$

By using Lasalle's invariant set theorem, system (8) is asymptotically stable. A more detailed discussion is in order to deal with the properties of this controller in the original coordinates, for which the reader is referred to ([6]).

IV. Visual-Servoing with Limited View-Angle

In this section, we introduce the hypothesis that the view-angle of the imaging system adopted in our vehicle is limited, as it happens with most economic cameras available on the market. The main practical constraint in the design of a control law for this case is related to the necessity of tracking features continuously. Indeed, while it is in principle possible to recover from a feature loss by replanning or by resorting to other sensorial information (such as e.g. odometry), this is usually to be avoided in the interest of simplicity and robustness.

Consider first the stabilization of the vehicle with the constraint that a single feature, placed at the origin of the desired frame $< W >$, is kept in view. Let the limited field-of-view be described by a symmetric cone centered in the optical axis Z_c with semi-aperture Δ. The feature-tracking constraint (for a single feature in the origin) is thus simply $|\beta| < \Delta$.

Consider application of the control law described in section III to the present problem, and the positive definite function $V(\phi, \beta) = \frac{\phi^2}{2} + \frac{\lambda\beta^2}{2}$. Also, consider an ellipse in the plane (ϕ, β) defined by $V \leq \frac{\lambda\Delta^2}{2}$. Along the controlled trajectories of the vehicle, one has $\dot V = -\lambda\beta^2$ which is negative semi-definite. Therefore, if the initial condition (ϕ_0, β_0) is within the ellipse, the evolution of (ϕ, β) remains indefinitely inside the ellipse (see fig. 3).

Observe that, for any initial condition (ϕ_0, β_0) such that the feature is visible (i.e., $\beta_0 < \Delta$), it is possible to choose a value for λ such that the evolution of β is always strictly bounded in the sector $(-\Delta, \Delta)$. Indeed, this can be obtained by putting $\lambda \geq \frac{{\phi_0}^2}{\Delta^2 - {\beta_0}^2}$ $(\lambda > 0)$. The actual choice of λ will be made depending on the extent of the expected range of possible initial conditions except for those having $|\beta_0| \geq \Delta$ (note that λ is not defined for $|\beta_0| = \Delta$).

Secondly, consider the case that the feature to be tracked is in a generic position R on the ${X_w}^+$ axis. The task is again to achieve docking at the origin with horizontal heading, by always maintaining the tracked feature in view. We point out explicitely that the different position of the features (which is obviously to be taken into account in practical applications) would not represent any additional difficulty in the omnidirectional sight case, while it implies more difficult maneuvering in the present setting.

For simplicity's sake, we replace here the state-space coordinate ϕ with $\alpha = \phi - \pi$, with $\dot\alpha = \dot\phi$. The constraint on the angle under which the camera views the tracked feature is now written as

$$ \gamma(\rho, \alpha, \beta) = \alpha - \beta - \arctan\frac{\rho \sin\alpha}{R + \rho\cos\alpha} \in [-\Delta, \Delta]. \qquad (9) $$

The application of the control law above described is not sufficient in general to solve this more complex problem, as the limitation of β through the choice of λ is no longer sufficient to ensure the FOV constraint (9). Indeed, with the control law (7), it is only possible to guarantee accomplishment of our goal

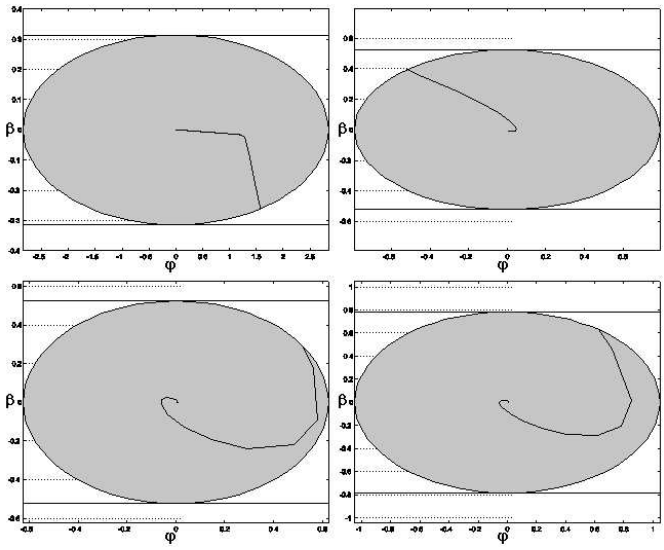

Fig. 3. Left: four examples of trajectories in an ellipse by the control(7).

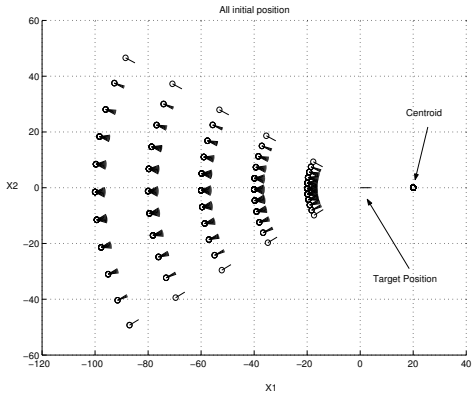

Fig. 4. The set of initial conditions from which the vehicle can be stabilized to the origin by a smooth controller without loosing track of a feature placed on the X_w axis, does not contain the origin in its interior.

(i.e., that the system is stabilized to the desired configuration while the FOV constraint is not violated), for a particular set $\Sigma \subset \mathbb{R}^+ \times S^2$ of initial conditions.

A description of Σ can be obtained by upper-bounding the absolute value of γ along the path defined by the stabilized dynamics (8), and reasoning along the lines above in the (α, β) plane. As a result, one gets the sufficient region depicted in fig. 4 which is comprised of initial configurations such that the whole X_w axis is within the camera's field-of-view. However, the desired configuration itself is on the boundary of Σ, hence no local stability can be claimed. To overcome this limitation, and obtain a stabilizing law that can be applied to any initial configuration, provided only that the FOV constraint is initially satisfied, we therefore use a more complex hybrid controller described in the next section.

V. Hybrid Visual-Feedback Controller

The basic idea to be applied in this section is rather simple, and is based on the fact that the Lyapunov-based control described in the previous section is not uniquely defined.

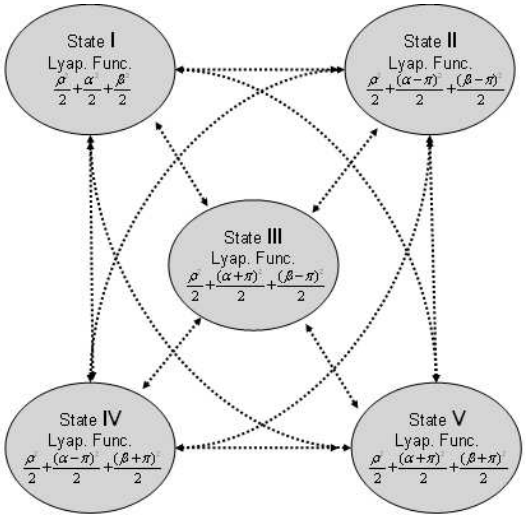

Fig. 5. Graphic representation of the hybrid controller. Each state has the corresponding Lyapunov function V_i defines in (10)

Rather, a whole family of controllers can be defined by simply redefining the control Lyapunov function candidate (see e.g. [15]). It can be expected that for such different candidates, the resulting stabilizing control laws and ensuing trajectories are different, and that switching among these control laws should be enabled when the FOV constraint is about to be violated. To precisely describe this approach, and to prove that it indeed produces a solution to our problem, we formalize the system using tools from the recently developed theory of *hybrid systems*. In their most simple description, hybrid systems are dynamical systems comprised of a finite state automaton, whose states correspond to a continuous dynamic evolution, and whose transitions can be enabled by particular conditions (*guards* or *jumps*) reached at by the continuous dynamics themselves ([16], [17], [18]). Consider the following five control Lyapunov functions (see fig. 5)

$$\begin{aligned} V_1(\rho,\alpha,\beta) &= \frac{\rho^2}{2} + \frac{\alpha^2}{2} + \frac{\beta^2}{2}, \\ V_2(\rho,\alpha,\beta) &= \frac{\rho^2}{2} + \frac{(\alpha-\pi)^2}{2} + \frac{(\beta-\pi)^2}{2}, \\ V_3(\rho,\alpha,\beta) &= \frac{\rho^2}{2} + \frac{(\alpha+\pi)^2}{2} + \frac{(\beta-\pi)^2}{2}, \\ V_4(\rho,\alpha,\beta) &= \frac{\rho^2}{2} + \frac{(\alpha-\pi)^2}{2} + \frac{(\beta+\pi)^2}{2}, \\ V_5(\rho,\alpha,\beta) &= \frac{\rho^2}{2} + \frac{(\alpha+\pi)^2}{2} + \frac{(\beta+\pi)^2}{2}. \end{aligned} \tag{10}$$

These definitions can be regarded as generated by defining the target configuration $\Phi_{goal} \in \mathbb{R}^+ \times S^2$ in five different ways, i.e. respectively $\Phi_{goal} = (0,0,0)$, $\Phi_{goal} = (0,\pi,\pi)$, $\Phi_{goal} = (0,-\pi,\pi)$, $\Phi_{goal} = (0,\pi,-\pi)$ and $\Phi_{goal} = (0,-\pi,-\pi)$. While the five definitions obviously correspond to the same final position and orientation of the vehicle, they engender different ways of reaching at the equilibrium ([15]), as illustrated by fig. 6. For compactness of notation, consider parameter vectors $\tilde{\beta} = [\beta, \beta-\pi, \beta-\pi, \beta+\pi, \beta+\pi]$, and $\tilde{\alpha} = [\alpha, \alpha-\pi, \alpha+\pi, \alpha-\pi, \alpha+\pi]$, so that (10) can be rewritten as $V_i(\rho,\alpha,\beta) = \frac{\rho^2}{2} + \frac{\tilde{\alpha}_i^2}{2} + \frac{\tilde{\beta}_i^2}{2}$. All the above Lyapunov functions have the same first term $\frac{\rho^2}{2}$ whose time derivative can be made non-positive by setting $u = \cos\beta$. The condition that also the second term of each Lyapunov function

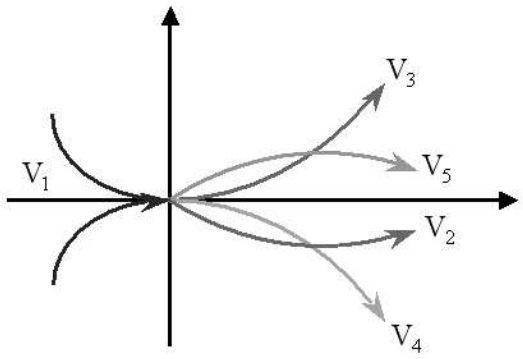

Fig. 6. Five different ways of converging to the desired configuration by the mobile robot under the five different control Lyapunov functions in (10).

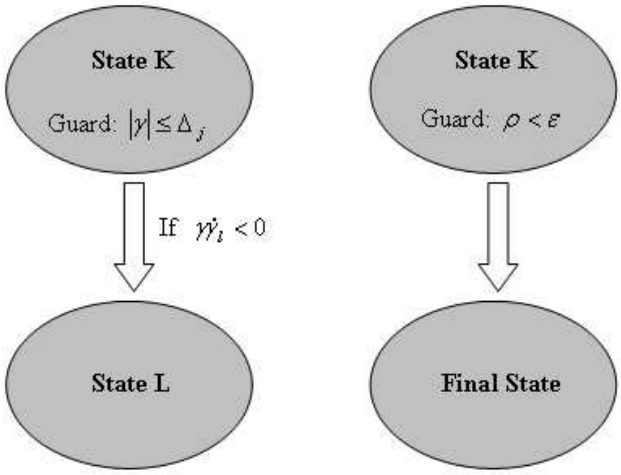

Fig. 7. Graphic representation of the jump sequences from a generic state K to the candidate state L if the guard is fired (left), and from each state of the previous hybrid automaton to the additional final state if the final position has been reached within an ϵ tolerance

is negative semidefinite implies that the ω control is chosen as

$$\omega_i = \lambda\tilde{\beta}_i + \frac{\sin\beta\cos\beta}{\tilde{\beta}_i}(\tilde{\alpha}_i + \tilde{\beta}_i), \tag{11}$$

with $\lambda > 0$ a constant parameter to be chosen. These five different control laws (parameterized by λ) define in turn five different controlled dynamics (analogous to (8)) that are globally asymptotically stable in the state manifold $\mathbb{R}^+ \times S^2$, although none of these alone can guarantee that the FOV constraint is satisfied throughout the parking maneuver.

A hybrid system with five discrete states is defined by the five dynamics laws above along with a switching law described by a jump event J_{hk} (jump from state h to state k), a commutation law, and an update law for λ (which could be formally regarded as an additional continuous state with trivial dynamics $\dot{\lambda} = 0$ and a reinitialization law at each control commutation).

The jump condition is triggered when, during the stabilization with one of the five control laws, the feature approaches the border of the field of view by a threshold $\Delta_j < \Delta$, i.e. when $|\gamma| \ge \Delta_j$, where γ is defined in (9).

When the jump condition is triggered in the state h, a choice is made among other available control functions in the other states k (see fig. 5) according to which guarantees that the feature is brought back towards the optical axis of the camera. In other terms, the control function is commuted to one such that $\gamma\dot{\gamma} < 0$ (see fig. 7). If multiple such choices exist, the one that maximizes some merit function is picked (in particular, we adopted the criterion that the control law ω_i is the one minimizing $\dot{V}_i$, although this choice is not of major consequence to the convergence of the method).

We first prove that the hybrid controller is deadlock free. Indeed, if along the evolution of the system (with any of the five controllers) γ does not reach the threshold value, then asymptotic convergence to the target configuration is granted by construction. On the other hand, it can be easily shown that in any configuration, there are always at least two possible different control laws among the five such that (by suitably setting λ), one has $\gamma\dot{\gamma} < 0$.

Indeed, by differentiating (9), one has $\dot{\gamma} = \eta - \omega$, with

$$\eta = \frac{\rho\cos\beta}{(R + \rho\cos\alpha)^2 + \rho^2\sin^2\alpha}[R\sin(\beta - \alpha) + \rho\sin\beta].$$

When $\gamma = \Delta_j$, the condition $\dot{\gamma} < 0$ is enforced if a commutation is made to a control function for which it holds

$$\lambda\tilde{\beta}_i > \eta - \frac{\sin\beta\cos\beta}{\tilde{\beta}_i}(\tilde{\alpha}_i + \tilde{\beta}_i). \tag{12}$$

Considering that, for any value of β, among the $\tilde{\beta}_i, i = 1, \ldots 5$ there are at least two positive values, it will be sufficient to choose one of them and a new λ such that

$$\lambda > \frac{\eta}{\tilde{\beta}_i} - \frac{\sin\beta\cos\beta}{\tilde{\beta}_i^2}(\tilde{\alpha}_i + \tilde{\beta}_i), \tag{13}$$

to ensure the condition on $\dot{\gamma}$. The case $\gamma = -\Delta_j$ is similar.

By the above argument, we have that the proposed hybrid control law guarantees satisfaction of the constraint provided only that it is satisfied at the initial configuration. It is now necessary to prove the convergence of the entire system to the desired configuration. Along the hybrid evolution, the distance of the vehicle from the origin, $\rho(t)$, is continuous with continuous first derivative, and non increasing (indeed, $\dot{\rho} = -\rho\cos^2\beta$ in all states). The set in which $\dot{\rho} = 0$ is given by

$$C_\rho = \{(\rho, \tilde{\alpha}_i, \tilde{\beta}_i) : \rho = 0\} \cup \{(\rho, \tilde{\alpha}_i, \tilde{\beta}_i) : \tilde{\beta}_i = \frac{\pi}{2} + k\pi\}.$$

However, it is easy to check that under the controlled dynamics and commutation laws above described, all configurations in C_ρ are not invariant. Hence, ρ converges asymptotically towards zero in every state of the hybrid system, while guaranteeing that the tracked feature remains in view.

It is important to notice that the control law defined thus far may generate switches among different control laws with an increasing frequency as ρ decreases. To avoid this phenomenon (sometimes referred to as the *Zeno behavior* in the hybrid

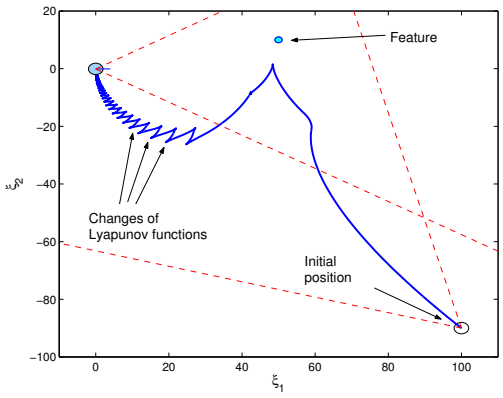

Fig. 8. Trajectory in the fixed frame $< W >$ of the unicycle. The restricted optical field of view of the camera and the starting position of the vehicle are represented.

system literature), it is sufficient to introduce a sixth state in the system automaton, into which a transition from any other state is allowed when $\rho < \epsilon$, where ϵ represents a tolerable value of the residual position error (see fig. 7). Once in this sixth state, the vehicle forward velocity u is set to zero, while the angular velocity is simply chosen as proportional to the error in the vehicle orientation, i.e. $\omega = k\gamma + \eta$. No exit condition is provided from this state (except for higher-level exceptions or functional interrupts). The practical stability of the proposed law is thus established to within a neighborhood $[\pm\epsilon, \pm\epsilon, \pm \arctan(\frac{\epsilon}{\sqrt{R^2-\epsilon^2}})]$ of the origin in the original coordinates (ξ_1, ξ_2, ξ_3).

It is important to also notice that in the case the hybrid controller is used the features can be in any position and not necessarily on the X_w axis. In such a case, if a feature is in position ${}^W P_i = {}^W [p_1^i, p_2^i, p_3^i]^T$ the corresponding γ_i can be evaluated as

$$\gamma_i(\rho, \alpha, \beta) = \alpha - \beta - \arctan \frac{{}^W p_3^i + \rho \sin \alpha}{{}^W p_1^i + \rho \cos \alpha} \in [-\Delta, \Delta]. \quad (14)$$

VI. Simulation and Experimental Results

The hybrid control technique proposed in the previous section has been used in simulation, to preliminarily address practically important concerns, such as e.g. computational load of the control law and compatibility with real-time operation, and to illustrate its behaviour. It is to be noticed, however, that virtually no parameter tuning is necessary for the correct operation of the proposed controller, which fact represents a distinct advantage of the proposed method.

In the simulation results presented in fig. 8, where the angle of view limit is set to $\Delta = \frac{\pi}{6}$, the unicycle achieves the goal notwithstanding the rather awkward initial position, with the selected feature situated between its start position and the desired one. Each cusp in the resulting trajectory corresponds to a switch among different states in the hybrid controller determined by the γ value. Chattering near the equilibrium illustrates the Zeno behavior, which is circumvented by the practically stabilizing controller described above.

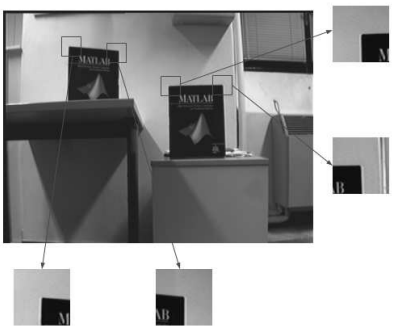

Fig. 9. Image grabbed from the target position, with the four selected control features shown in detail.

To validate the practicality and portability of the proposed techniques, two different experimental platforms have been used, with different quality of components (and cost).

The first experimental setup was comprised of a TRC LabMate vehicle, equipped with an analogical monochromatic camera Jai CVM-50 [19] placed on the robot so that a vertical axis through the camera pinhole intersects the wheel axis in the midpoint. The camera allows for a $\Delta = \pi/6$ semi-aperture of the optical cone, while a threshold of $\Delta_j = \pi/8$ was used in the experiment. The controller is implemented under Linux on a 300MHz PentiumII PC equipped with a Matrox MeteorI frame grabber. The XVision library (see [20]) is used to compute optical flow and to track features. The hardware communication between the robot and the PC is performed by a RS-232 serial cable. A few procedures have been used to improve the signal-to-noise ratio in grabbed images, as e.g. multiple temporal windowing and filtering of grabbed images. To avoid the intrinsic analytical singularities on the inversion of the perspective projection, a semi-heuristic technique has been implemented, called *Feature Migration*, that consists in mapping features (in both current and target images) away from the middle axis, to reject mismatches in the camera calibration parameters and feature heights.

In the experiment, four features from the scene are used to implement the algorithm (see fig. 9). Although the theory above described has only been proved for a single feature, we successfully applied a slightly modified version to the problem of keeping multiple features in view. The target image, recorded in a preliminary phase of the experiment, is reported in fig. 9. Images grabbed from the robot camera in the initial, offset configuration and at the end of the visually-servoed parking maneuver are shown in fig. 10, along with ground-reference views showing the experimental environment (see also Extensions 1,2 and 3).

For the second set of experiments, a low-cost apparatus was employed, to highlight the robustness and applicability potential of the proposed technique. The experimental setup was comprised of a K-Team Koala vehicle [21], equipped with a cheap Kodak EZ200 web-cam [22] placed on the front part of the robot platform. The vehicle has two symmetric rows of three wheels on its sides, each actuated by a single low-resolution stepper-motor actuator: the construction implies that slipping and skidding of some of the wheels occurs whenever

Fig. 10. External views (left column) and subjective images (right column) as taken from the vehicle, in the initial configuration (top row) and in the final configuration (bottom row), after reaching convergence under the proposed visual feedback control scheme. The bottom right image should be compared with the target image in fig. 9.

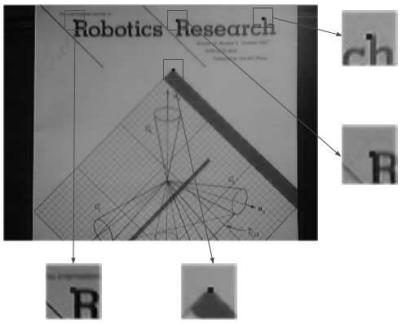

Fig. 11. Desired image and selected features for the second experiment.

the vehicle moves along a curved trajectory. Such conditions make it hard to use odometry for localization and control, and strongly motivates the use of visual servoing. The controller is implemented under Windows XP on a 1130MHz Pentium III laptop mounted on-board. The VisSDK [23] and Intel OpenCV [24] libraries were used to compute optical flow and to track features. The hardware communication between the robot and the laptop is performed by a RS-232 serial cable. Image processing techniques similar to those described in the previous experiment were implemented. Because of the appreciable distortion of the camera, the FOV threshold was set to a narrow $\Delta_j = \pi/16$ in this experiment. The target image is reported in fig. 11, with the four selected features used to implement the algorithm. The initial configuration of the vehicle in the environment, and the corresponding image grabbed from the robot camera are reported in fig. 12 (left and right images, respectively). Notice that the robot has to move along a direction parallel to the wheel axle to reach the target position, hence the parking problem can be expected to involve rather complicated maneuvering. For this experiment, the guard condition to enter the final state of the hybrid automaton (see fig. 7) was set to $\epsilon = 5mm$. The image grabbed at the end of the visually-servoed parking maneuver is shown in fig. 12, right. The trajectory followed by the vehicle during the

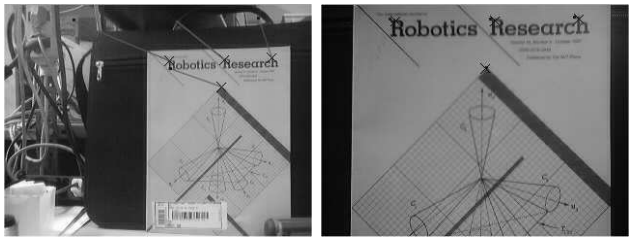

Fig. 12. Left: Image grabbed from the starting position. Right: Image grabbed from the final position (to be compared with fig. 11.

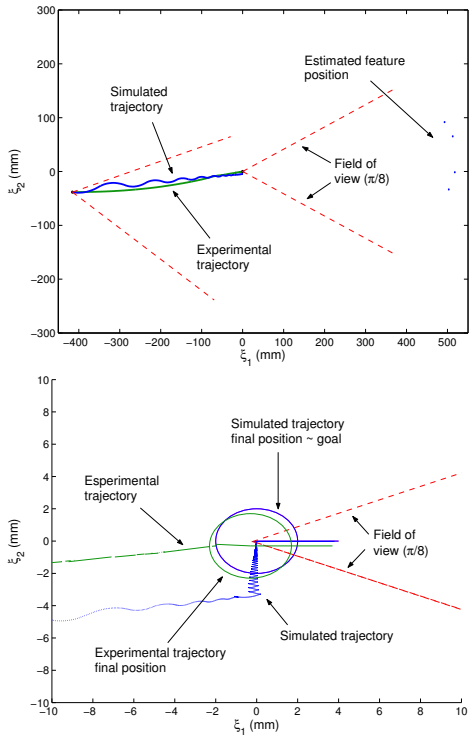

Fig. 13. Experimental and simulated trajectories followed by the vehicle in the fixed frame $< W >$. A zoom on the final configuration is reported in the bottom graph.

docking experiment is reported in fig. 13 (see also Extensions 4 and 5), along with the trajectory resulting from simulation of the controlled system from identical initial conditions. It can be observed that the final configuration reached in simulation is very close to the goal, while experimental data show a larger residual position error. Furthermore, it is interesting to note that experimental trajectories differ from simulations, especially in the region closest to the goal (fig. 13, bottom), as the former appear to be smoother. These discrepancies can be explained by the presence of substantially more noisy data in localization (requiring filtering of raw odometric and vision data), and by the presence of vehicle and tire mechanics, which effectively act as low-pass filters between command inputs and executed trajectories. Data on feature trajectories on the image plane are reported in fig. 14, top, showing their convergence to the desired positions and the switching phenomena under the hybrid controller different control laws. The bottom part of fig. 14 shows simulated trajectories of the same four

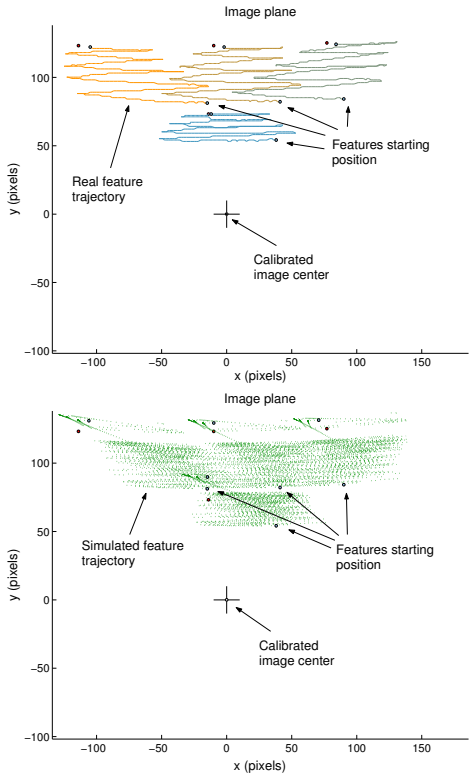

Fig. 14. Trajectories of the selected features in the image plane: experimental (top) and simulated (bottom).

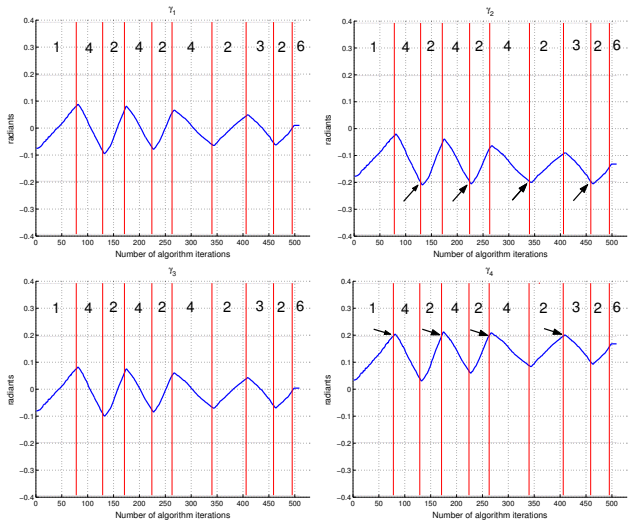

Fig. 15. Evolution of the four γ angles, showing when guard conditions are triggered in the hybrid controller.

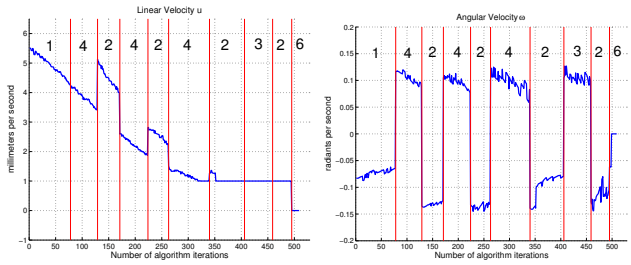

Fig. 16. Control inputs (linear and angular velocities) to the vehicle during the second experiment. Switchings in the hybrid controller invert the direction of the angular velocity, to recover the position of features approaching the field-of-view limit.

features. Again, experiments behave much more smoothly, albeit reaching a worse approximation of the desired goal than simulations. The time evolution of the values of the four γ angles in Fig. 15, illustrates satisfaction of the FOV constraint, and shows when guard conditions are triggered in the hybrid controller. Different control Lyapunov functions $V_1 - - V_6$ used in different phases of the experiment are indicated. Finally, the control signals (linear and angular velocity) applied to the vehicle, and the evolution of the vehicle state in the working coordinates (α, β, ρ) and in the original coordinates (ξ_1, ξ_2, ξ_3), are shown in figs. 16, 17, and 18, respectively. It is worthwhile to notice that, while in the working coordinates the convergence of α and β is heavily affected by noise in the region where ρ is small, this effect is rejected to an acceptable level in the original coordinates, due to the "zooming" nature of the coordinate transform used.

VII. Conclusion

In this paper, we have proposed a control algorithm for parking wheeled vehicles. To address economicity of applications, realistic assumptions on the nature and quality of the vehicles and of their sensorial equipment have been considered. Accordingly, the control scheme uses exclusively information from conventional cameras fixed on-board the vehicle. The algorithm deals with practical limitations imposed by limits on the field of view of such sensors, by adopting a switching strategy, whose convergence is proven by modern hybrid control techniques. Practical implementation of switching control laws implies in general some difficulties, such as related to for instance sensor inaccuracies, delays in commutation and possible Zeno-type phenomena (infinitely fast switching). However, simple countermeasures have been adopted (accepting a tolerance on stabilization and adding a corresponding final state to the hybrid automaton) leading to an acceptable behaviour. Experiments on two widely different platforms have been executed, assessing both the practicality and portability of the proposed algorithms.

Appendix

Index to Multi-Media Extensions The multi-media extensions to this article can be found online by following the hyperlinks from www.ijrr.org.

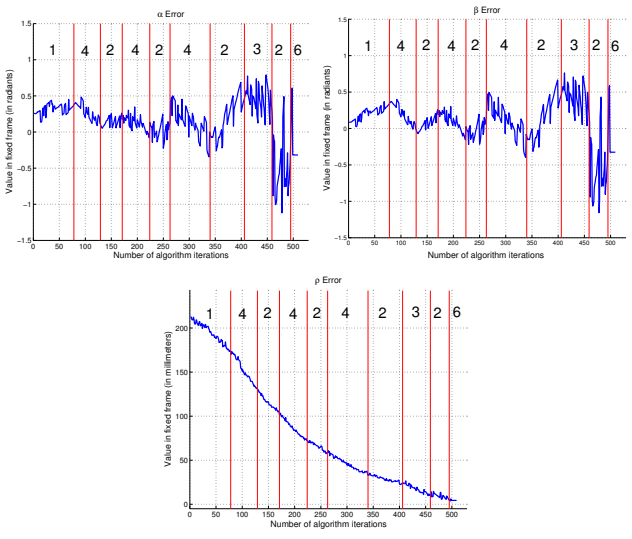

Fig. 17. Evolution of the working coordinates α, β and ρ. Sensor noise on the angular displacements is apparent especially in the final phase, when the distance from the target position is small.

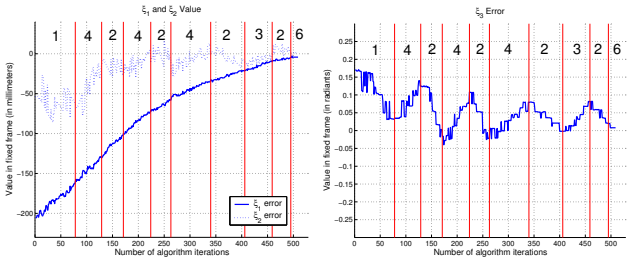

Fig. 18. Evolution of the original vehicle coordinates, ξ_1, ξ_2 and ξ_3. Good convergence to the desired values and immunity to sensor noise are exhibited.

Extension	Media Type	Description
1	Video	First Experiment: General view
2	Video	First Experiment: Subjective View from the Robot
3	Video	First Experiment: Ground-based View
4	Video	Second Experiment: General View
5	Video	Second Experiment: Subjective View from the Robot

REFERENCES

[1] R. Brockett, "Asymptotic stability and feedback stabilization," in *Differential Geometric Control Theory*, M. Brockett and Sussmann, Eds. Boston, U.S.: Birkhauser, 1983, pp. 181–191.

[2] G. Campion, B. d'Andrèa Novel, and G. Bastin, "Controllability and state feedback stabilization of nonholonomic wheeled mechanical systems," in *Advanced Robotic Control*. Springer-Verlag, 1991, pp. 106–124.

[3] C. C. de Wit and O. Sordalen, "Exponential stabilization of mobile robots with nonholonomic constraints," *IEEE Transactions on Robotics and Automation*, vol. 37, no. 11, Nov. 1992.

[4] D. Tilbury and A. Chelouah, "Steering a three-input nonholonomic system using multi-rate controls," in *European Control Conference*, June 1993, pp. 1428–1431.

[5] P.Morin and C. Samson, "Application of backstepping techniques to the time-varying exponential stabilization of chained form systems," INRIA Research Report, Tech. Rep. 2792, 1996, sophia-Antipolis.

[6] G. Casalino, M. Aicardi, A. Bicchi, and A. Balestrino, "Closed loop steering and path following for unicycle–like vehicles: a simple lyapunov function based approach," *IEEE Robotics and Automation Magazine*, vol. 2, no. 1, pp. 27–35, March 1995.

[7] B. d'Andréa Novel, G. Campion, and G. Bastin, "Control of nonholonomic wheeled mobile robots by state feedback linearization," *International Journal of Robotics Research*, vol. 14, no. 6, pp. 543–559, December 1995.

[8] J. P. Hespanha, "Single camera visual servoing," in *Proc. IEEE Int. Conf. on Decision and Control*, 2000, pp. 2533–2538.

[9] D. Tsakiris, P. Rives, and C. Samson, "Applying visual servoing techniques to control nonholonomic mobile robots," in *International Conference on Intelligent Robots and Systems*, September 1997, workshop on "New Trends in Image-based Robot Servoing".

[10] K. Hashimoto and T. Noritsugu, "Visual servoing of nonholonomic cart," in *Proc. Int. Conf. on Robotics and Automation*, April 1997, pp. 1719–1724.

[11] F. Conticelli, D. Prattichizzo, F. Guidi, and A. Bicchi, "Vision-based dynamic estimation and set-point stabilization of nonholonomic vehicles," in *Proc. IEEE Int. Conf. on Robotics and Automation*, San Francisco, CA, USA, 2000, pp. 2771–2776.

[12] Y. Mezouar and F. Chaumette, "Path planning in image space for robust visual servoing," IRISA-INRIA Rennes, Tech. Rep., 1998.

[13] R. Hartley and A. Zisserman, *Multiple view geometry in computer vision*. Cambridge University Press, 2000.

[14] M. Ollis, H. Herman, and S. Singh, "Analysis and design of panoramic stereo vision using equi-angular pixel cameras," Robotics Institute, Carnegie Mellon University, Pittsburgh, PA, Tech. Rep. CMU-RI-TR-99-04, January 1999.

[15] G. Casalino, M. Aicardi, A. Bicchi, and A. Balestrino, "Closed-loop steering and path following for unicycle-like vehicles: a simple liapunov function based approach," in *Proc. IFAC Int. Symposium on Robot Control*. Capri: Elsevier Science, Oxford, UK, 1994.

[16] M. Branicky, "Multiple lyapunov functions and other analysis tools for switched and hybrid systems," *IEEE Trans. on Automatic Control*, vol. 43, no. 4, pp. 475–482, 1998.

[17] T. Henzinger and S. S. S. (eds.), *Hybrid Systems: Computation and Control*, ser. Lecture Notes in Computer Science. Springer, 1998, vol. 1386.

[18] J. M. Schumacher and A. J. van der Schaft, *Introduction to Hybrid Dynamical Systems*. Springer-Verlag London, 1999.

[19] *Jai CVM-50 Monochrome Camera*, http://www.compumodules.com/imaging/cameras_list.shtml.

[20] G. D. Hager and K. Toyama, "X vision: A portable substrate for real-time vision applications," *Computer Vision and Image Understanding: CVIU*, vol. 69, no. 1, pp. 023–037, 1998.

[21] *K-Team Koala Robot*, http://www.k-team.com/robots/koala/index.html.

[22] *Kodak EZ200 Web-Cam*, http://www.photo.net/ezshop/product?product_id=2371.

[23] *Microsoft VisSDK*, http://msdn.microsoft.com/library/sdkdoc/vissdk/vissdk.htm.

[24] *Intel Open Source Computer Vision Library*, http://www.intel.com/research/mrl/research/opencv/.